Synthesis and magnetic characterization of $TmCo_2B_2C$



2009 J. Phys.: Condens. Matter 21 046007

(http://iopscience.iop.org/0953-8984/21/4/046007)

J. Phys.: Condens. Matter **21** (2009) 046007 (9pp) doi:10.1088/0953-8984/21/4/046007

# Synthesis and magnetic characterization of $TmCo_2B_2C$

**M ElMassalami[1], R E Rapp[1], F A B Chaves[1], R Moreno[1], H Takeya[2], B Ouladdiaf[3], J W Lynn[4], Q Huang[4], R S Freitas[5] and N F Oliveria Jr[5]**

[1] Instituto de Fisica, Universidade Federal do Rio de Janeiro, Caixa Postal 68528, 21945-972 Rio de Janeiro, Brazil
[2] National Institute for Materials Science, 1-2-1 Sengen, Tsukuba, Ibaraki 305-0047, Japan
[3] Institut Laue-Langevin, BP 156, 38042 Grenoble Cedex 9, France
[4] NIST Center for Neutron Research, National Institute of Standards and Technology, Gaithersburg, MD 20899-6102, USA
[5] Instituto de Física, Universidade de São Paulo, Rua do Matão 187 Travessa R, Cidade Universitária, 05315-970 Sao Paulo, SP, Brazil

Received 7 July 2008, in final form 23 September 2008
Published 8 January 2009
Online at stacks.iop.org/JPhysCM/21/046007

**Abstract**

A new quaternary intermetallic borocarbide $TmCo_2B_2C$ has been synthesized via rapid-quench of an arc-melted ingot. Elemental and powder-diffraction analyses established its correct stoichiometry and single-phase character. The crystal structure is isomorphous with that of $TmNi_2B_2C$ ($I4/mmm$) and is stable over the studied temperature range. Above 7 K, the paramagnetic state follows modified Curie–Weiss behavior ($\chi = C/(T - \theta) + \chi_0$) wherein $\chi_0 = 0.008(1)$ emu mol$^{-1}$ with the temperature-dependent term reflecting the paramagnetism of the Tm subsystem: $\mu_{\rm eff} = 7.6(2)\ \mu_{\rm B}$ (in agreement with the expected value for a free $Tm^{3+}$ ion) and $\theta = -4.5(3)$ K. Long-range ferromagnetic order of the Tm sublattice is observed to develop around ~1 K. No superconductivity is detected in $TmCo_2B_2C$ down to 20 mK, a feature which is consistent with the general trend in the $RCo_2B_2C$ series. Finally, the influence of the rapid-quench process on the magnetism (and superconductivity) of $TmNi_2B_2C$ will be discussed and compared to that of $TmCo_2B_2C$.

(Some figures in this article are in colour only in the electronic version)

## 1. Introduction

The magnetic ordering temperature of a $Tm^{3+}$ sublattice in a thulium-based intermetallic compound is, in general, lower than that of its isomorphous heavy rare-earth-based counterparts of the same series [1]. One usually attributes such a lowering to a smaller de Gennes factor, $(g-1)^2 J(J+1)$, assuming that parameters such as electronic structure are not modified across the isomorphous series. On the other hand, for Tm-based compounds that belong to a family of a different series, electronic properties (such as the position of the Fermi level within the density of states curve, the derivative of the density of states, etc) do change, and such a change can significantly modify the type, and critical point of the magnetic order. Such features are well documented in, say, the $RM_2$ family (R = magnetic rare earth, M = 3d transition metal) [2–5]: for the $TmM_2$ compounds, the critical temperature of each member depends critically on the type of M, but for each $RM_2$ series it is always lower than that of the corresponding heavy R-isomorphs.

Another illustration which is of relevance to this work is the case of the heavier members of the borocarbide family $RM_2B_2C$. For the $RNi_2B_2C$ series, the Néel temperatures ($T_N$) scale reasonably well with the de Gennes factor [6–8]; moreover, both $T_N$ (1.5 K) and the de Gennes factor (1.17) of $TmNi_2B_2C$ are the lowest. In contrast, the critical points $T_C$ of the isomorphous series $RCo_2B_2C$ do not show this scaling. Furthermore, $T_C$ of $TmCo_2B_2C$ has not, so far, been reported, but based on an extrapolation of $T_C$ within the phase diagram of $RCo_2B_2C$ ($T_C$ versus the de Gennes factor) it is expected to be 2 K [9]. However, this would contradict the observed trend that $T_C$ s of the heavier members of $RCo_2B_2C$ are not higher than those of the corresponding $RNi_2B_2C$. This question has not been addressed before due to difficulties

 

in synthesizing and stabilizing a single-phase $TmCo_2B_2C$ compound. This work reports on the successful preparation as well as the structural and physical characterization of single-phase $TmCo_2B_2C$ samples. The obtained results confirm that its $T_C$ is indeed no higher than that of $TmNi_2B_2C$.

Two findings are of special interest for an understanding of superconductivity and magnetism, and their interplay, in the borocarbide family. First, no sign of superconductivity is observed down to 20 mK; such a result, together with the non-superconductivity of $YCo_2B_2C$ [9, 10], indicates that the quench of the superconductivity in $RCo_2B_2C$ is related to the unfavorable spin fluctuation process (for the particular case of $TmCo_2B_2C$, there is, in addition, the pair-braking ferromagnetic (FM) order). Secondly, the long-range order of the localized 4f moments of $TmCo_2B_2C$ does not appear to be a spin density wave as in the case of $TmNi_2B_2C$; rather, we argue that a FM state is consistent with the results of the magnetization, specific heat, and neutron diffraction. These findings will be demonstrated and discussed in section 3. Before that we describe, in section 2, the synthesis process and show how the stoichiometry and the single-phase character of the rapid-quenched (rq) $TmCo_2B_2C$ and $TmNi_2B_2C$ samples were verified. An evaluation of the influence of the rate of the rq process on the studied physical properties of $TmCo_2B_2C$ (section 2) together with a detailed comparison of the properties of a normally prepared, non-quenched (nq) $TmNi_2B_2C$ with those of a rq-$TmNi_2B_2C$ (section 2) would allow us to extract the dominant influences of the rq process.

## 2. Experimental details

### *2.1. rq $TmCo_2B_2C$*

A starting sample with a stoichiometry of $TmCo_2B_2C$ was prepared by a conventional arc-melt procedure under a highly pure (99.999%) argon atmosphere. The obtained product, when tested with x-ray diffraction, showed a multi-phase pattern. This same product, shaped into balls with diameters around 3–5 mm, was remelted and directly rapid-quenched by hitting it with a copper hammer [11]. The final product is a single-phase $TmCo_2B_2C$ in the form of thin flakes (50–100 $\mu$m thickness). Once obtained, the sample is stable in air and does not need any special care during the handling or storing process, at least within an interval of months.

In contrast to the $RNi_2B_2C$ series [12, 13] or even to other $RCo_2B_2C$ members [9], the rq process is essential for the synthesis of $TmCo_2B_2C$. Figure 1 shows the diffractograms of two samples of $TmCo_2B_2C$ prepared at different quenching rates (the one with a faster quench rate is enriched with $^{11}B$). These diffractograms, together with results from various measuring techniques, reveal that the rq process drastically diminishes the amount of impurity phases and as such leads to noticeable changes in the physical properties (see below, in particular figure 4). All measurements reported below were carried out on the same as-prepared, rapid-quenched $^{11}B$-enriched batch: conventional annealing (often followed for the borocarbide samples) leads to a surge of additional contamination.

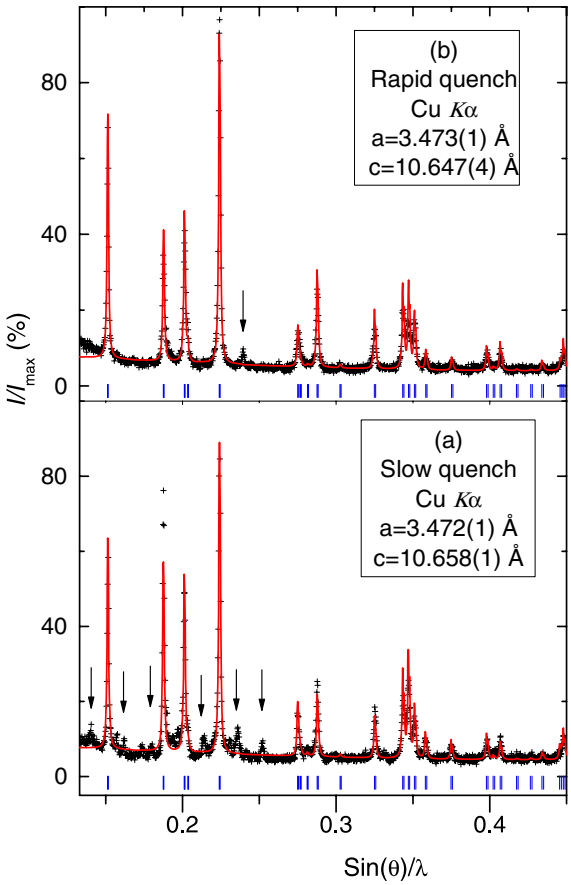


**Figure 1.** Room-temperature x-ray diffractograms (Cu K$\alpha$) of (a) slow-quenched and (b) rapid-quenched $TmCo_2B_2C$. Rietveld analysis (solid lines) shows that the lattice parameters are hardly affected by the variation of the quench rate. Nevertheless, the impurity content is noticeably suppressed. On comparison with the neutron diffractograms (see later), allowance should be made for the difference in the $f$-factors.

The elemental analysis of both rq-$TmCo_2B_2C$ and rq-$TmNi_2B_2C$ is shown in table 1. The Tm, Co, and B contents were determined by the induction coupled plasma analysis, while the C was determined by the process of carbon combustion followed by infrared absorption analysis. Table 1 also shows the cell parameters as obtained from room-temperature x-ray diffraction analysis (figure 1(b)). As can be verified, these results (in particular that of B and C) do confirm the correct stoichiometry of the $TmCo_2B_2C$ samples.

The crystal structure was studied by x-ray diffraction (room temperature) and neutron diffraction (0.36 K $< T <$ 30 K). Physical characterizations were carried out with the following techniques: magnetization ($M(T, H)$, 0.5 K $< T <$ 30 K, $H <$ 150 kOe), dc susceptibility ($\chi_{dc}(T) = M/H$, 0.5 K $< T <$ 300 K, $H \leqslant$ 10 kOe), ac susceptibility ($\chi_{ac}(T)$, 0.02 K $< T <$ 20 K, $f =$ 200–1000 Hz, $h_{ac} <$ 10 Oe), and specific heat ($C(T)$, semi-adiabatic, 0.1 K $< T <$ 15 K). Neutron diffraction was carried out at two different sites: (i) the Institut Laue-Langevin (ILL, Grenoble, France) using the D2B diffractometer (3 K $\leqslant T \leqslant$ 30 K) with a wavelength of $\lambda = 1.595$ Å, and (ii) the National Institute of Standards and Technology (NIST, Gaithersburg, MD, USA) using the high-

**Table 1.** The molar ratios of the $^{11}$B-enriched, rapid-quenched $TmCo_2B_2C$ and $TmNi_2B_2C$ samples. The calculations are based on the weight percentage data (normalized to the Tm content) and using the following atomic weights: Tm = 168.934 21(3), Co = 58.933 20(1), Ni = 58.6934, $^{11}$B = 10.995 (99.5% enriched from Eagle Pitcher Ind. Inc.), B = 10.811(5), and C = 12.011(1). The room-temperature cell parameters of $TmCo_2B_2C$, as obtained from XRD analysis (see figure 1), are $a = 3.473(1)$ Å, $c = 10.647(4)$ Å. For $TmNi_2B_2C$, see table 2.

| Compound | Ratio | Tm | Co | Ni | B | C |
|---|---|---|---|---|---|---|
| $TmCo_2B_2C$ | % | 52.2(1) | 36.3(1) | — | 6.69(1) | 3.81(1) |
| | Molar | 1 | 1.993(5) | — | 1.97(3) | 1.03(3) |
| $TmNi_2B_2C$ | % | 52.8(1) | — | 36.0(1) | 6.39(1) | 3.77(1) |
| | Molar | 1 | — | 1.962(6) | 1.86(3) | 1.00(3) |

resolution powder diffractometer ($\lambda = 2.0787$ Å, $T = 0.36$ K) and the BT-9 triple axis instrument with a pyrolytic graphite monochromator and filter ($\lambda = 2.359$ Å, 0.48 K $\leqslant T \leqslant$ 4.5 K). Data were also collected on the new BT-7 triple axis spectrometer using the position sensitive detector in diffraction mode. For these neutron measurements a sample weighing 0.66 g was used.

### 2.2. *rq-$TmNi_2B_2C$*

Intended as a helpful guide in the evaluation of how much the properties of $TmCo_2B_2C$ are being influenced by the rq process, we also investigated the physical properties of a rq-$TmNi_2B_2C$ sample and compared the results with those for the reported nq-$TmNi_2B_2C$ sample. It is recalled that a nq-$TmNi_2B_2C$ sample shows typical second-order-type superconducting and magnetic phase transitions occurring, respectively, at $T_c = 11$ K and $T_N = 1.5$ K [14, 15]. We synthesized rq-$TmNi_2B_2C$ via an identical preparation procedure to the one used for $TmCo_2B_2C$; the resulting sample has been studied by room-temperature XRD, specific heat, and magnetization measurements. The cell parameters and the paramagnetic Curie–Weiss (CW) behavior (see table 2) reflect slight modifications which may be related to the rq process and a slight depletion in B content. It is noted that the rq process does not induce any noticeable moment on the Ni sublattice.

Figure 2 shows that both the magnetic and superconducting order of $TmNi_2B_2C$ do survive the rq process (only that $T_N$ and $T_c$ are lowered to 1.2 and 10 K, respectively), suggesting that the intrinsic forces that govern these cooperative phenomena are much stronger than the quench-induced disordering effects. Nevertheless, the rq process has modified substantially the structure of the curves within the transition region: the width of the superconducting phase transition (figure 2(a)) is substantially increased while the height (width) of the magnetic phase transition is strongly reduced (increased), to the extent that the magnetic transition is manifested as a weak, broadened event; the λ-type magnetic transition of the nq sample is being transformed by the rq process into an almost featureless event; in this case the phase change, in contrast to the nq case, is evidenced in the features of the first-order derivative: thus the rq process may modify the character and type of the magnetic phase transition. As no hysteresis effects were

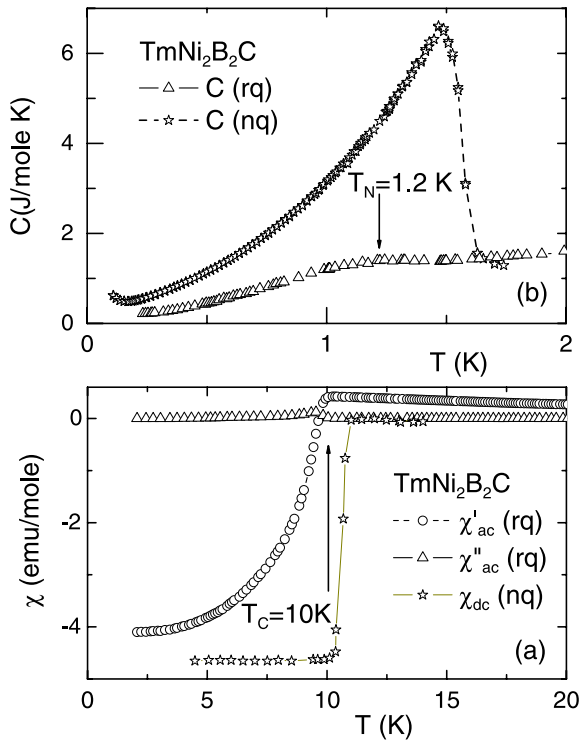


**Figure 2.** (a) Low-temperature, low-field ac ($\chi_{ac}$) and dc ($\chi_{dc}$) susceptibilities of $TmNi_2B_2C$. $\chi_{ac}$ ($H_{ac} = 1$ Oe, $f = 500$ Hz) is measured on a rq sample while $\chi_{dc}$ ($H_{dc} = 10$ Oe) was measured by Cho *et al* [14] on a nq sample. (b) The total specific heats of rq- and nq-$TmNi_2B_2C$ samples. The latter is taken from Movshovich *et al* [15]. Note the large broadening of the superconducting and magnetic transitions of the rq samples.

observed, the assignment of a first-order character to this phase transition is not unambiguous. At any rate, it can be safely concluded that the superconducting (and to some extent the magnetic) features of both rq- and nq-$TmNi_2B_2C$, except for the region neighboring the critical temperature, are practically similar. It is then concluded that the tetragonal $TmNi_2B_2C$ structure, in sharp contrast with $TmCo_2B_2C$, is a low-temperature phase. Nevertheless, the observation that both isomorphs have almost the same structural–chemical properties suggests that the overall effect of the rq process on the physical properties of $TmCo_2B_2C$ would not differ much from the trend observed in $TmNi_2B_2C$; in particular as the rq process did not drastically modify the intrinsic physical properties of $TmNi_2B_2C$, then both features of $TmCo_2B_2C$ (the non-superconductivity and the FM mode, see below) are considered to be intrinsic properties that are not strongly influenced by the rq process.

## 3. Results and discussion

The analysis of the powder diffractograms (figure 3 and table 3) indicates that $TmCo_2B_2C$ crystallizes in the tetragonal $LuNi_2B_2C$-type structure which, within the experimental accuracy, is stable over the range 0.36 K $\leqslant T \leqslant$ 300 K. In comparison with isomorphous $TmNi_2B_2C$, the introduction of Co reduces the $a$-parameter and elongates the $c$-axis length

**Table 2.** Comparison between the room-temperature cell parameters ($a$, $c$), the $z$ parameter indicating the position of the B atom (the positions of the other atoms are fixed by symmetry), and the paramagnetic Curie–Weiss (CW) parameters (figures not shown) of the rapid-quenched and non-quenched sample of $TmNi_2B_2C$. For the non-quenched sample, the cell parameters are taken from Lynn *et al* [8] while the CW parameters are from Cho *et al* [14].

| $TmNi_2B_2C$ | $a$ (Å) | $c$ (Å) | $z$ | $p_{\rm eff}$ ($\mu_B$) | $\theta$ (K) |
|---|---|---|---|---|---|
| Rapid-quenched | 3.4857(9) | 10.5609(27) | 0.3519 | 7.6(1) | −7.5(2) |
| Non-quenched | 3.4866(2) | 10.5860(5) | 0.3598(2) | 7.54(2) | −11.6(4) |

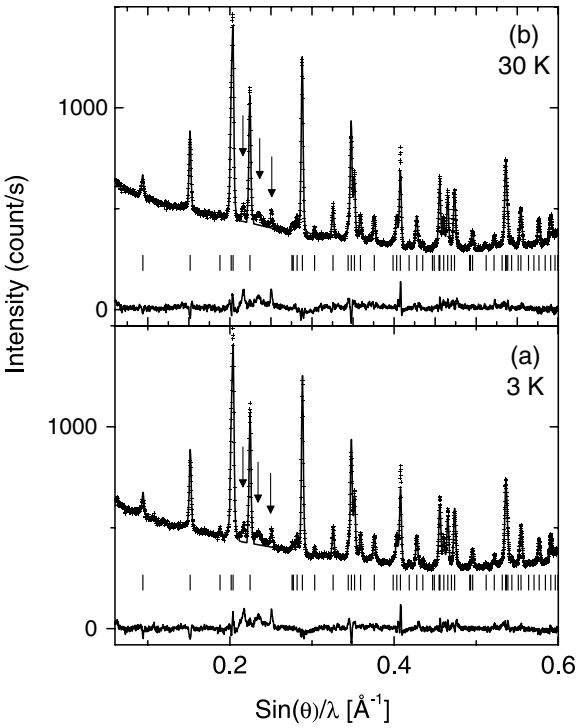


**Figure 3.** Neutron powder diffractograms of $TmCo_2B_2C$ measured on the D2B (ILL) diffractometer at (a) 3 K and (b) 30 K. Note the very weak impurity lines at $\sin(\theta)/\lambda = 0.217$, 0.234, and 0.251 Å$^{-1}$ (see figure 1). The intensity of the strongest impurity line relative to that of the main phase amounts only to 4%.

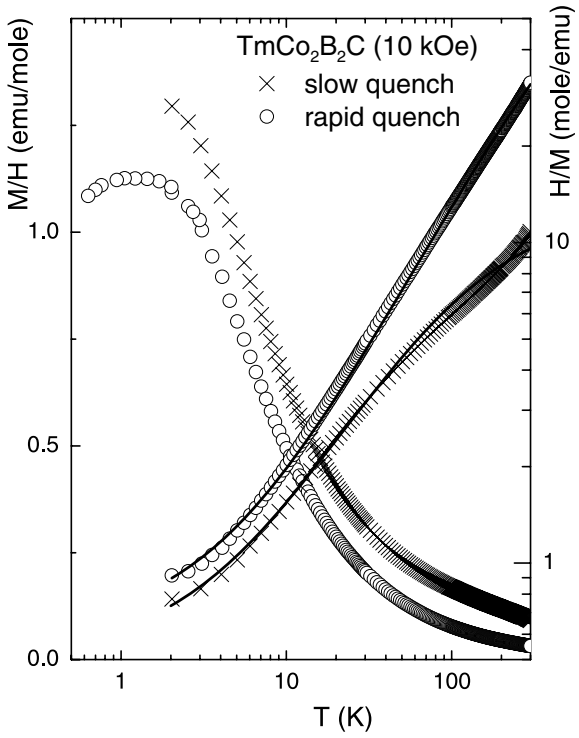


**Figure 4.** Temperature-dependent $\chi_{\rm dc} = M/H$ curves at $H = 10$ kOe of $TmCo_2B_2C$. The temperature axis is logarithmic so as to emphasize the low-temperature part. The influence of the rate of the quenching process is demonstrated by comparison with a slow-quenched sample (see figure 1). The reciprocal $\chi_{\rm dc}$ (right ordinate, logarithmic) for the rq sample (represented by circles) is well described by the modified CW behavior which is shown as solid lines (see the text).

**Table 3.** Cell parameters ($a$, $c$) and the B atom $z$-parameter of $TmCo_2B_2C$ at selected temperatures. The experimental diffractograms and the theoretically calculated patterns are shown in figures 3 and 9. In the Rietveld analysis of the diffractograms, the thermal parameters were found to be the same as those of $TmNi_2B_2C$ given in Lynn *et al* [8] while the occupation parameters gave similar values to those obtained from elemental analysis (see table 1).

| $T$ (K) | $a$ (Å) | $c$ (Å) | $z$ |
|---|---|---|---|
| 30 | 3.4684(2) | 10.6411(6) | 0.3597(2) |
| 3 | 3.4681(2) | 10.6413(7) | 0.3596(2) |
| 0.36 | 3.4689(2) | 10.6438(9) | 0.3587(3) |

but it induces no drastic shift in the B $z$-parameter (no particular significance is attributed to the observation that the $z$-parameters of both rq samples are 2% different from the nq-$TmNi_2B_2C$). It is reassuring that the obtained cell parameters, when plotted together with those of the other $RCo_2B_2C$ compounds, evolve linearly with the effective metallic radius of the R atom (see figure 2 of [9]).

### *3.1. Magnetic susceptibilities (ac and dc)*

Thermal evolution of the isofield dc susceptibilities of the rq-$TmCo_2B_2C$, $\chi_{\rm dc} = M/H$ (figure 4) down to 7 K, follows faithfully the modified CW behavior $\chi_{\rm dc}(T) = C/(T - \theta) + \chi_0$, wherein $\mu_{\rm eff} = 7.6(2)\ \mu_B$, $\theta = -4.5(3)$ K, and the temperature-independent paramagnetic (TIP) contribution $\chi_0 = 0.008(1)$ emu mol$^{-1}$. Similar high-temperature, modified CW paramagnetism is also manifested in the zero-field $\chi_{\rm ac}(T > 7\ {\rm K}) = \partial M/\partial H$ curve (figure 5). $\chi_{\rm dc}(T)$ of a slow-quenched (sq) $TmCo_2B_2C$ (also shown in figure 4) is higher in value and is not well described by the modified CW law. Based on the structural analysis, the difference between these two curves is related to the content of the contamination which, in turn, is governed by the speed of the quenching rate (see figure 1): a faster rate leads to a reduction in contamination and, consequently, to a lowering of the magnetic susceptibility,

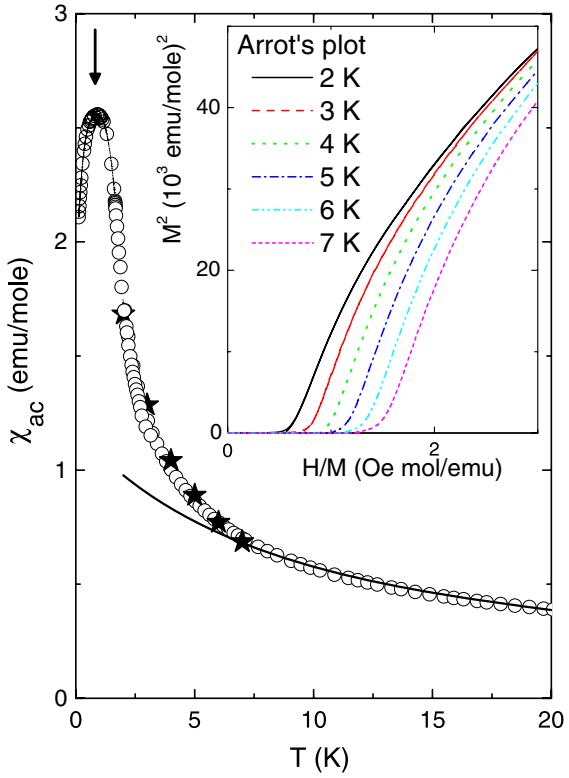


**Figure 5.** Thermal evolution of the zero-field $\chi_{ac}(T) = \partial M/\partial H$ of the rq-$TmCo_2B_2C$. The solid line represents a fit to the same modified CW relation as in figure 4. The stars represent $(M/H)_{H\to 0}$ extrapolated from the Arrott plots which are shown in the inset: the agreement indicates that the influence of the magnetic impurities within this range of temperatures is negligible.

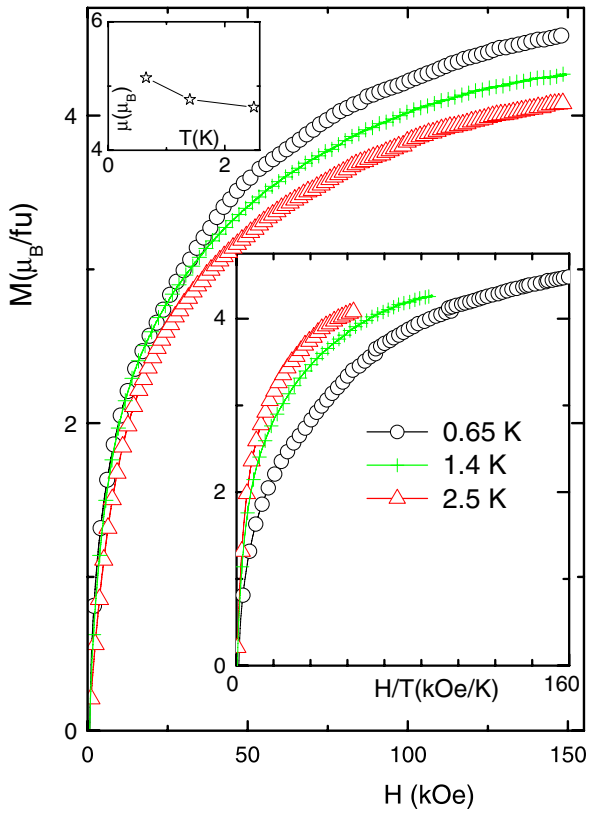


**Figure 6.** Magnetization isotherms $M(H)$ of $TmCo_2B_2C$ at different temperatures The lower-right inset shows the $M$ versus $H/T$ curves while the upper-left inset shows the saturated moment obtained from $\lim_{1/H\to 0} M(H)$. The lines are a guide to the eye (see the text).

in particular $\chi_0$. It is expected that on the limit of a faster quench, there would be no impurity contribution and $\chi_0$ would be much smaller but non-vanishing, since $\chi_0$ of $YCo_2B_2C$ is non-zero [16]. Such a limit $\chi_0$ may be due to a van Vleck-type contribution or an exchange-enhanced Pauli susceptibility. The admixture of high-lying orbitals into the ground state of the $Tm^{3+}$ ion can be ruled out, since no such effect is observed in $TmNi_2B_2C$ [14] (not even in the rq samples; see table 2). But such TIP is common in the cubic Laves $RCo_2$ phases [2, 3] wherein $\chi_0 \approx 0.004$ emu $mol^{-1}$. Though the above arguments as well as the similar argument on $YCo_2B_2C$ [16] suggest that such an additional $\chi_0$ may be related to a modification in the electronic structure of the 3d subband (as a result of the introduction of the Co atoms), a final statement on this $\chi_0$ should wait for further analysis.

As the temperature is lowered towards and below the liquid helium point, both $\chi_{dc}(T)$ (figure 4) and $\chi_{ac}(T)$ (figure 5) manifest a rapid increase, go through a peak, and afterward drop weakly downwards. Considering that $\chi_{ac}(T)$ has an accentuated peak with a maximum at 0.8(1) K and that at this point $\chi_{dc}(T, 10\ \text{kOe})$ starts to decrease, such a point is taken to indicate a magnetic phase transition (see below).

### *3.2. Magnetization*

Magnetization isotherms (figure 6) show that even for a field of 150 kOe the magnetic moment per unit formula reaches only $4.5 \pm 0.2\ \mu_B$ ($T = 0.65$ K) which is 65% of the value expected for a free $Tm^{3+}$ ion. Such a high-field susceptibility is attributed to the magnetic response of the Co subsystem. The total moment saturation is estimated from the extrapolation $\lim_{1/H\to 0} M(H)$: the saturated moment (upper-left inset of figure 6) increases smoothly as the temperature is decreased. On the other hand, the $M$ versus $H/T$ curves (lower-right inset of figure 6) reveal that the isotherms at 1.4 and 2.5 K almost collapse on each other but that of 0.65 K is distinctly different. This observation supports our earlier arguments that $TmCo_2B_2C$ orders magnetically with an onset point lower than 1.4 K: within the paramagnetic state, all $M(H/T)$ curves follow the same Brillouin function and as such collapse on each other, while below $T_C$ the rapid development of the ordered moment ensures that all of the $M(H/T)$ isotherms are distinctly different from one another and, in particular, from all paramagnetic isotherms.

Chang *et al* [17] observed that the moment of $TmNi_2B_2C$ increases as the temperature decreases; namely $\mu(1.2\ \text{K}) = 3.74\ \mu_B$ and $\mu(50\ \text{mK}) = 4.8\ \mu_B$. Comparing these features with those of figure 6, it is inferred that the magnitude and thermal evolution of the moments of both isotherms are similar, which suggests a similarity in the low-lying crystalline electric field (CEF) level scheme. As such it is expected that the orientation of the Tm moment should be along the $c$-axis just as observed in $TmNi_2B_2C$. The observed difference in the strength of the $Tm^{3+}$ moment of the two isomorphs may be due

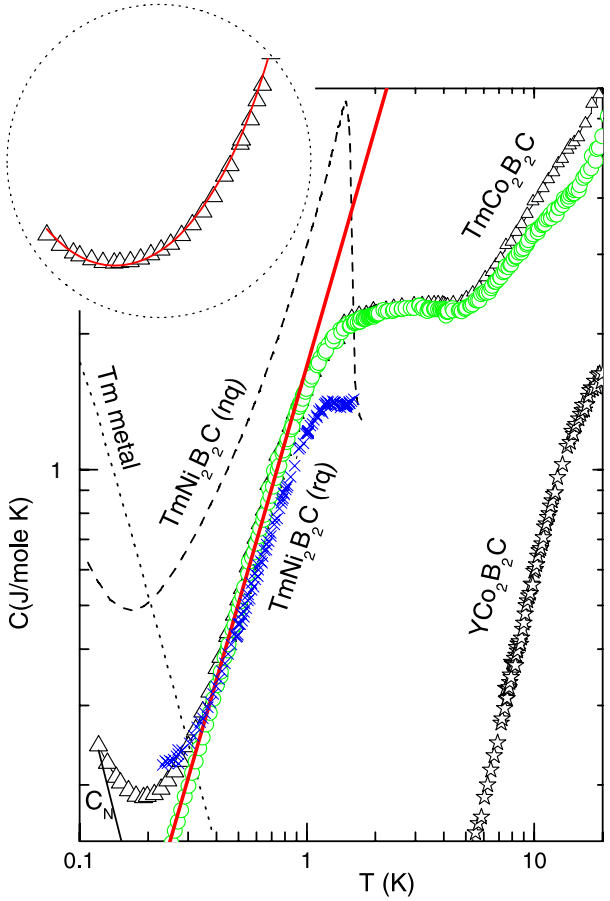


**Figure 7.** The specific heat curve (triangles) of $TmCo_2B_2C$. For comparison, we include the specific heat of $YCo_2B_2C$ (stars, [16]), the non-quenched $TmNi_2B_2C$ (dashed line, [15]), the rapid-quench $TmNi_2B_2C$ (cross, figure 1), and (only the nuclear contribution of) the Tm metal (dotted line, [20]). The magnetic contribution (circles) and the empirical function $C_M(T) = 1.7T^{\frac{7}{4}}$ J mol$^{-1}$ K$^{-1}$ (thick solid line) are also indicated (see the text). The inset shows an expansion of the low-temperature tail of the total specific heat of $TmCo_2B_2C$ (triangles) together with $C_{tot} = C_{ep}$ ($YCo_2B_2C$) $+ 0.035T^{-2}$ $+ 1.7T^{\frac{7}{4}}$ J mol$^{-1}$ K$^{-1}$ (solid line).

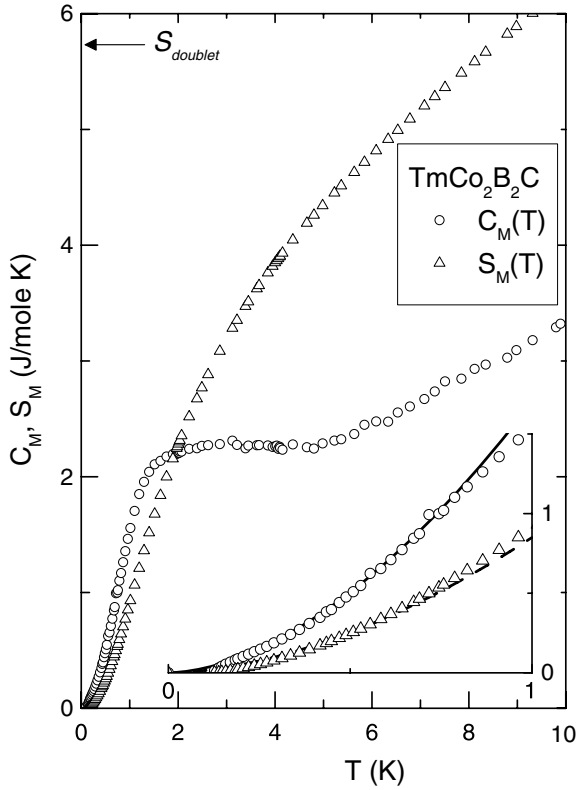


**Figure 8.** The magnetic contribution to the specific heat (circles) and magnetic entropy (triangles) of $TmCo_2B_2C$. The expected entropy for a doublet is shown as a horizontal arrow. The inset shows, on an expanded scale, the experimental curves together with their low-temperature fits: $C_M(T) = 1.7T^{\frac{7}{4}}$ J mol$^{-1}$ K$^{-1}$ (solid line) and $S_M(T) = 0.85T^{\frac{7}{4}}$ J mol$^{-1}$ K$^{-1}$ (dashed line).

to a slight variation in the CEF effects. The influence of rq on the site-occupation may lead to a reduction or even a complete collapse of the Tm moment (as argued by Mulder *et al* [18, 19] to explain the reduction of the Tm moment in $TmNi_2B_2C$).

The low-field part of the $M(H, 0.65\ \text{K})$ curve of figure 6 does not manifest those characteristic features (such as convex curvature at a spin flop event) which can be taken as indicative of an AFM ground state; instead it shows a monotonic and steep increase which is typical of a forced magnetization of a FM-like state. It is not uncommon in the magnetism of the intermetallics that the character of the magnetic ground state is different from that suggested by the sign of the CW temperature.

### *3.3. Specific heat*

The zero-field $C(T)$ curve of $TmCo_2B_2C$ is shown in figure 7. The low-temperature part of the total $C(T)$ is largely due to the magnetic contribution, $C_M(T)$, which is obtained after subtracting the contributions due to both the diamagnetic reference ($YCo_2B_2C$, [9]) and the nuclear interaction ($C_N \approx 3.5$ T$^{-2}$ mJ mol$^{-1}$ K$^{-1}$). It is interesting to note that the associated hyperfine interaction (and the electronic magnetic moment) is much smaller than that of Tm metal ($C_N \approx 26.8$ T$^{-2}$ mJ mol$^{-1}$ K$^{-1}$) [20], but closer, as expected, to that of $TmNi_2B_2C$ ($C_N \approx 4.8$ T$^{-2}$ mJ mol$^{-1}$ K$^{-1}$) [15].

Figures 7 and 8 show that $C_M(T < 0.8\ \text{K}) = 1.7T^{\frac{7}{4}}$ J mol$^{-1}$ K$^{-1}$; above 0.8 K it turns slowly into a plateau which extends up to 5 K; above this temperature it resumes a monotonic increase but at a slower rate. This power-type thermal evolution of $C_M(T)$ (with an exponent being close to $\frac{3}{2}$) is consistent with what one would expect from a magnon contribution of a FM ordered state wherein the dispersion relation is quadratic and the anisotropic field is vanishingly small [21, 22].

The magnetic entropy (figure 8) evolves as $S_M(T < 0.8\ \text{K}) = 0.85T^{\frac{7}{4}}$ J mol$^{-1}$ K$^{-1}$, increases steadily for $T > 0.8$ K, and approximates the doublet-value R ln(2) only above 8 K. As all contributions from the Co subsystem has already been subtracted, this entropy contribution must then be due solely to the Tm subsystem and as such the lowest-lying two levels of $Tm^{3+}$ are separated from the highest ones by an energy gap which must be much higher than 8 K: indeed inelastic neutron scattering on isomorphous $TmNi_2B_2C$

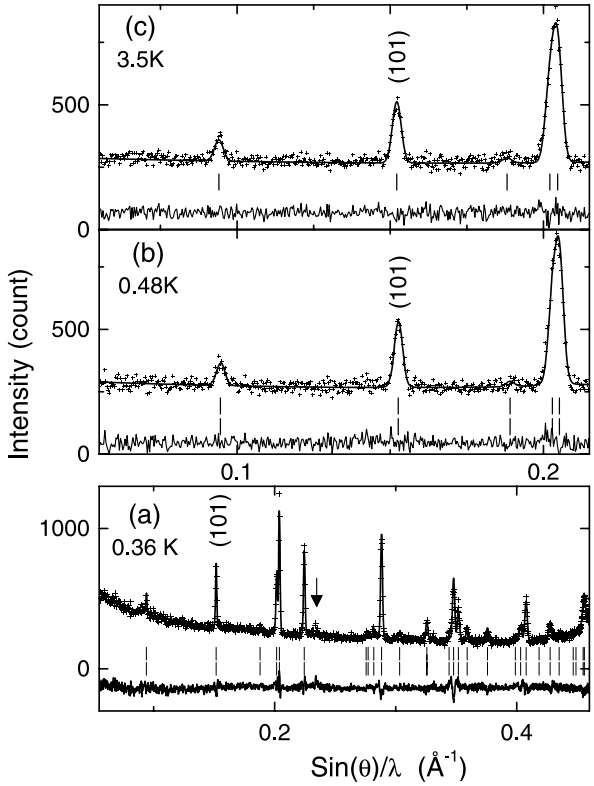


**Figure 9.** Neutron diffractograms of $TmCo_2B_2C$, measured at (a) the NIST high-resolution diffractometer, $\lambda = 2.0787$ Å, and ((b), (c)) the NIST triple axis diffractometer $\lambda = 2.359$ Å. The small vertical arrow indicates an impurity peak (see figures 1 and 3). A noticeable increase in the low angle intensities can be observed in the lower panel but not in the upper panels: this suggests that this broadening is instrument dependent and not due to small angle scattering arising from magnetic or structural disorder induced by the rapid-quench process.

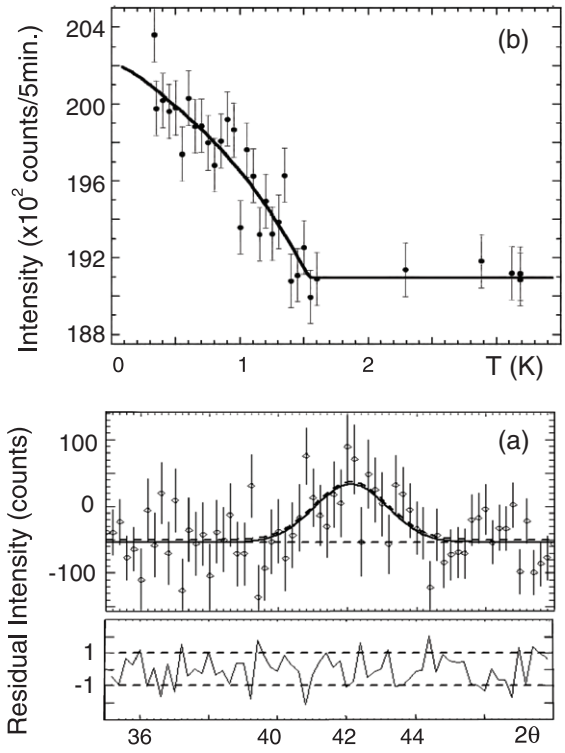


**Figure 10.** (a) The difference pattern of the (101) peak obtained after subtracting the intensities measured at 4.0 K from those measured at 0.45 K. The line is a Gaussian fit to the experimental points (the residual graph represents the difference between the fit and the data). (b) Thermal evolution of the intensity of the (101) Bragg peak. Each point represents a measurement of the peak using a single setting of the position sensitive detector on BT-7. The solid curve is a fit to mean field theory; this gives a critical temperature of 1.54(8) K. Error bars in this figure are statistical and represent one standard deviation.

showed that the doublet ground state is separated from the first excited state by 30 K [23–26]. We have carried out preliminary inelastic neutron measurements on BT-7 to search for crystal field excitations in $TmCo_2B_2C$. We did not find any sharp excitations up to an energy transfer of 20 meV, but we did observe at 4.0 K a distribution of scattering (not shown) that appeared quasi-elastic, employing an energy resolution of 1.0 meV. The wavevector and temperature dependence of this scattering indicated that it was magnetic in origin, and fitting with a Lorentzian distribution gave a half width $\Gamma = 3.9(4)$ meV. Further studies are under way.

As seen in figure 2(b), the $C(T)$ curve of the rq $TmNi_2B_2C$ manifests the magnetic phase transition as a broadened and weak magnetic event. Along the same line of reasoning, the shoulder-like region in figures 7 and 8 is considered to be the region within which the magnetic phase transition of $TmCo_2B_2C$ sets in (see the last comment in section 2.2). Then the critical temperature is taken to be the point of the maximum slope which is found to be 0.8 K, in excellent agreement with the considerations of figures 4–6.

### *3.4. Neutron diffraction*

The high-resolution neutron diffractograms (figure 9) have been measured on BT-1 down to 0.36 K using a He3 cryostat and for as low an angle as possible. Within the measured temperature range and experimental accuracy, no additional Bragg peaks that might be associated with magnetic order are observed. We therefore carried out diffraction measurements using the high-intensity/coarse resolution thermal triple axis instruments BT-9 and BT-7 to search for magnetic order. Within the angular range up to a scattering angle of 65°, the only significant change in intensity was observed for the (101) Bragg peak, as shown by the difference plot in figure 10(a). The temperature dependence of the intensity of this peak is shown in figure 10(b), and the increase at lower temperatures indicates that magnetic order has developed. The solid curve is a fit of mean field theory to the data, which indicates that the magnetic ordering temperature is 1.54 K; this critical point (though determined from mean field analysis which is not well suited for such a determination) is nearly twice the value estimated from the susceptibility (figure 5) and the specific heat (figure 7). Considering that the rq process is observed to induce a drastic broadening in the transition region (see figure 2), then it is most probable that the difference in the values of the transition point is due to the fact these techniques differ in their frequency window.

The observation of a magnetic contribution at the (101) peak suggests that the magnetic wavevector is (000). It is

emphasized that the weak impurities do not influence this analysis since we used the subtraction method (see figure 10). Below we argue that the only magnetic structure which is compatible with this (000) wavevector is the FM state. Such a conclusion is consistent with the above mentioned arguments about the forced magnetization (figure 6) and the magnon contribution of the specific heat (figure 7). As the crystal structure is body-centered tetragonal (no orthorhombic distortion is expected since magnetostriction effects are weak) with only one Tm atom per primitive cell, then no order of the Tm sublattice can be antiferromagnetic. However, there are two Co atoms per primitive cell and as such an AFM order may develop, but this should be discarded since there are no magnetic moments on the Co sublattice (see above). Thus it is concluded that this magnetic order must be due to the FM order of the Tm sublattice: it is recalled that both the saturated and effective moments are in excellent agreement with those found for $TmNi_2B_2C$. It is worth adding that our recent studies show that the manifestation of a FM state in $TmCo_2B_2C$ is not unusual: a FM state is common among the magnetic $RCo_2B_2C$ compounds [27] such as $TbCo_2B_2C$, $DyCo_2B_2C$, and $HoCo_2B_2C$.

On comparing the obtained results for $TmCo_2B_2C$ with those for $TmNi_2B_2C$, it is evident that their magnetic ground states are different: the former manifests a collinear FM state while the latter orders into a modulated spin density wave. This difference is attributed to the difference in the indirect exchange couplings which in turn is due to the difference in the electronic structures. It is recalled that there is a clear difference between the electronic structure of $LuNi_2B_2C$ and $LuCo_2B_2C$ [28]. On the other hand, the observation that their magnetic moments are similar is an indication that the CEF properties of the $Tm^{3+}$ ions have not been greatly modified by the rq process or by the interchange of the 3d atoms.

$TmCo_2B_2C$ shows no trace of superconductivity in the ac susceptibility (down to 20 mK), the specific heat (down to 100 mK), or the preliminary resistivity curves measured down to 20 mK (not shown). It is recalled that none of the reported members of the $RCo_2B_2C$ series is a superconductor [9], not even $YCo_2B_2C$ in spite of having a Sommerfeld constant and Debye temperature that are almost equal to those of superconducting $YNi_2B_2C$; $YCo_2B_2C$ manifests spin fluctuation features [16], a property assumed to be unfavorable for the onset of the superconductivity. These spin fluctuations (associated with the Co sublattice) together with the presence of the FM state (associated with the Tm sublattice) are detrimental to the presence of the superconductivity in $TmCo_2B_2C$.

## 4. Conclusion

A single-phase $TmCo_2B_2C$ has been successfully stabilized via the rapid-quench process. Its crystal structure is isomorphous to that of the body-centered tetragonal $TmNi_2B_2C$. The paramagnetic properties are characterized by a modified CW behavior while the low-temperature features are dominated by an ordering of $Tm^{3+}$ moments. Based on the character of the low-temperature magnon contribution to the specific heat, the characteristic feature of the low-temperature forced magnetization, and the analysis of the magnetic contribution to the neutron diffractograms, it is inferred that the magnetic order of the Tm sublattice is FM. At 0.65 K and under an applied magnetic field of 150 kOe, the $Tm^{3+}$ moment is observed to reach $4.5 \pm 0.2\ \mu_B$; though only 65% of the value expected for a free $Tm^{3+}$ ion, this value is only 6% lower than the moment of $TmNi_2B_2C$. It is concluded then that the CEF effects in both isomorphs are similar. Finally, no superconductivity is observed in $TmCo_2B_2C$ down to 20 mK: a feature attributed to the presence of the spin fluctuation in the Co subsystem and the FM ordering of the Tm sublattice.

## Acknowledgments

We acknowledge partial financial support from the Brazilian agencies CNPq (485058/2006-5) and Faperj (E-26/171. 343/2005). Identification of commercial equipment in the text is not intended to imply recommendation or endorsement by National Institute of Standards and Technology. We would like to thank Jiying Li for his assistance with the data analysis using the position sensitive detector on BT-7.

## References

[1] Coqblin B 1977 *The Electronic Structure of Rare-Earth Metals and Alloys: The Magnetic Heavy Rare-Earth* (New York: Academic)
[2] Bloch D and Lemaire R 1970 *Phys. Rev.* B **2** 2648
[3] Bloch D, Edwards D M, Shimizu M and Voiron J 1975 *J. Phys. F: Met. Phys.* **5** 1217
[4] Cyrot M and Lavagna M 1979 *J. Physique* **40** 763
[5] Inoue J and Shimizu M 1988 *J. Phys. F: Met. Phys.* **18** 2487
[6] Eisaki H, Takagi H, Cava R J, Batlogg B, Krajewski J J, Peck W F, Mizuhashi K, Lee J O and Uchida S 1994 *Phys. Rev.* B **50** R647
[7] Cho B K, Canfield P C and Johnston D C 1996 *Phys. Rev. Lett.* **77** 163
[8] Lynn J W, Skanthakumar S, Huang Q, Sinha S K, Hossain Z, Gupta L C, Nagarajan R and Godart C 1997 *Phys. Rev.* B **55** 6584
[9] ElMassalami M, DaCosta M S, Rapp R E and Chaves F A B 2000 *Phys. Rev.* B **62** 8942
[10] El Massalami M, Chagas E F and Rapp R E 2001 *J. Magn. Magn. Mater.* **226–230** 1058
[11] Takeya H, Togano K, Sung Y S, Mochiku T and Hirata K 2004 *Physica* C **408** 144
[12] Siegrist T, Zandbergen H W, Cava R, Krajewski J J and Peck W F 1994 *Nature* **367** 254
[13] Siegrist T, Cava R, Krajewski J J and Peck W F 1994 *J. Alloys Compounds* **216** 135
[14] Cho B K, Xu M, Canfield P C, Miller L L and Johnston D C 1995 *Phys. Rev.* B **52** 3676
[15] Movshovich R, Hundley M F, Thompson J D, Canfield P C, Cho B K and Chubukov A V 1994 *Physica* C **227** 381
[16] El Massalami M, Borges H A, Takeya H, Rapp R E and Chaves A 2004 *J. Magn. Magn. Mater.* **279** 5
[17] Chang L J, Tomy C V, Paul D M and Ritter C 1996 *Phys. Rev.* B **54** 9031
[18] Mulders A M, Gubbens P C M and Buschow K H J 1996 *Phys. Rev.* B **54** 14 963
[19] Mulders A M, Gubbens P C M, Gasser U, Baines C and Buschow K H J 1998 *Phys. Rev.* B **57** 10 320

[20] Holmstrom B, Anderson A C and Kruis M 1969 *Phys. Rev.* **188** 888
[21] El Massalami M, Rapp R E, Chaves F A B, Takeya H and Chaves C M 2003 *Phys. Rev.* B **67** 224407
[22] El Massalami M, Rapp R E and Takeya H 2003 *Studies in High Temperature Superconductors* vol 45, ed A Narlikar (New York: Nova Science)
[23] Gasser U, Allenspach P, Mesot J and Furrer A 1997 *Physica* C **282–287** 1327
[24] Gasser U, Allenspach P, Fauth F, Henggeler W, Mesot J, Furrer A, Rosenkranz S, Vorderwisch P and Buchgeiste M 1996 *Z. Phys.* B **101** 345
[25] Rotter M, Sierks C, Loewenhaupt M, Freudenberger J and Schober H 2001 *Rare Earth Transition Metal Borocarbides (Nitrides): Superconducting, Magnetic and Normal State Properties* (*NATO Advanced Research Workshop*) ed K H Müller and V Narozhnyi (Dordrecht: Kluwer–Academic) pp 137–53
[26] Gasser U, Allenspach P, Furrer A and Mulders A M 1998 *J. Alloys Compounds* **257–277** 587
[27] ElMassalami M, Moreno R, Saeed R M, Chaves F A B, Chaves C M, Takeya H, Ouladdiaf B and Amara M 2008 *J. Phys.: Condens. Matter* submitted
[28] Coehoorn R 1994 *Physica* C **228** 331